Applicability of the Fracture Flow Interface to the Analysis of Piping in Granular Material

Silvia Bersan[*1], Cristina Jommi[2], André Koelewijn[3], Paolo Simonini[1]
[1]University of Padua, [2]Delft University of Technology, [3]Deltares
*Corresponding author: silvia.bersan@dicea.unipd.it

Abstract: Piping is a kind of internal erosion that occurs under water retaining structures lying on a sandy soil. In an attempt to reproduce the growth of erosion channels in sand, a small scale physical model has been set up in the laboratory and a finite element model that reproduces the physical model has been developed. This paper presents the comparison among modelling strategies, from which emerged that laminar flow in the erosion channel can be modelled using Darcy's law and the Fracture Flow interface. A first use of the numerical model is also presented, concerning the optimization of the size of the small-scale set-up.

Keywords: internal erosion, piping, groundwater flow, Fracture Flow.

1. Introduction

The structural integrity of water retaining structures as river dikes, sea dikes and dams is threatened by internal erosion: the removal of soil particles due to high seepage forces. Several terms have been used in the literature to classify the principal mechanisms of internal erosion, generating sometimes little confusion. In this paper the word 'piping' refers to the development of erosion channels (*pipes*) in a sandy soil laying underneath a water retaining structure with an impervious (clayey or concrete) base (Figure 1).

The erosion process starts at the downstream side of the structure where the flow lines converge.
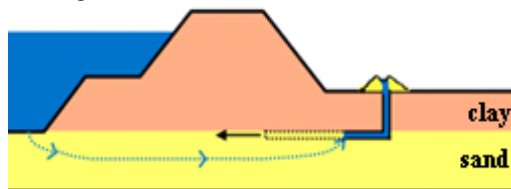

Figure 1. Pipe development under an impervious water retaining structure.

The pipes are initially very small and have cross-sections shaped as elongated rectangles, with a thickness of a few millimeters and a width of a few centimeters. They subsequently develop backwards and when they reach the upstream side they enormously widen and the structure can collapse quickly [1].

Despite not many cases of piping-induced collapse have been documented, due to the difficulty in recognizing clearly the traces of the mechanism before and even after the collapse occurred, piping is nowadays considered a big threat for dikes and dams [2, 3].

In the last decades, sand box models have been set up in an attempt to reproduce the growth of erosion channels in sand and to improve the existing rules for the prediction of piping [4]. Sand box models consist of a rigid box filled with sand, a fluid supply system and measuring devices. Usually the box is made of a transparent material to follow the movement of the particles at the walls.

Research is also focusing on the design of monitoring systems capable of detecting the occurrence of piping at an early stage. Traditionally, pore pressures are measured, while monitoring systems under study are based on the measurement of temperature [5], electrical potential and acoustic emissions [6].

A sand box model has been be set up by the authors, aimed at testing a monitoring system based on temperature measurements. COMSOL has been chosen as a modelling tool to investigate issues related to the design of the facility and to analyze, subsequently, the results of the tests, as it allows effective coupling of groundwater flow and heat transfer in three dimensional geometries.

Theoretical and numerical modelling of piping so far has been mainly two-dimensional [7, 8]. However the three-dimensional nature of the erosion process has been recently highlighted and is being studied [9]. 3D modelling is also important when investigating the effect of an erosion channel on the physical quantities that can be measured in its surroundings. This is a

key point in the design of a monitoring system.

In this work only the hydraulic modelling of the problem is addressed.

2. Governing equations

Fluid flow in porous media is typically modelled using Darcy's law

$$\mathbf{u} = -\frac{\kappa}{\mu}(\nabla p + \rho g \nabla z) = -\frac{\kappa}{\mu}\rho g \nabla H \quad (1)$$

In the above formulas $\mathbf{u}$ is a vector describing the rate of flow through a surface element of unit area, also named Darcy velocity or specific discharge, κ is the permeability of the porous mass, μ is the fluid viscosity, p is the pore pressure, ρ is the fluid density, g is the acceleration of gravity, z is the elevation head, H is the hydraulic head and ∇ denotes the gradient operator.

Flow in piping channels is described by Navier-Stokes equations and has been traditionally considered laminar, due to the small size of the pipes and the limited velocities that can be reached in the pipe under the hydraulic loads applied to small and medium water retaining structures. When the inertial term can be neglected, Navier-Stokes equations take the name of Stokes equations and can be written in the following simplified form:

$$\nabla p = \mu \Delta \mathbf{u} + \mathbf{F} \quad (2)$$

where $\mathbf{F}$ is a vector that accounts for gravity and/or other volume forces.

Eq. (1) and (2) are solved in combination with the continuity equation:

$$\nabla \cdot (\rho \, \mathbf{u}) = 0 \quad (3)$$

The inherent order difference between Darcy's law and Navier-Stokes equations generates a difficulty at the interface between the porous medium and the pipe. Darcy's law is indeed of fist-order in spatial derivatives so that only one boundary condition can be applied, either on the pressure or on the velocity component normal to the boundary. If the normal velocity is assigned, the other components of the velocity have arbitrary values at the wall. To overcome this difficulty some authors used an empirical relationship that links the interface velocity and the interface velocity gradient through a 'slip coefficient' thus obtaining a 'slip boundary condition' [10].

The approach adopted by COMSOL consists in using Brinkman equations to describe the flow in the porous matrix and Navier-Stokes equations in the free space. Brinkman [11] modified Eq. (1) by adding a term:

$$\nabla p = -\frac{\mu}{\kappa}\mathbf{u} + \mu \Delta \mathbf{u} + \mathbf{F} \quad (4)$$

Eq. (4) can also be derived from Navier-Stokes equations through a volume-averaging technique [12]. It has the advantage of approximating Eq. (1) for low values of κ and Eq. (2) for high values of κ. Being of second-order in spatial derivatives, Brinkman equations allow two boundary conditions to be set at the interface with the pipe: not only the continuity of the pressure field is guaranteed but also the continuity of all the velocity components.

3. Modelling strategies

The hydraulic module will be combined in the future with the thermal module in a transient analysis. It is therefore paramount to keep the computational cost related to the hydraulic part as low as possible. 3D finite element discretization of Navier-Stokes and Brinkman equations requires to solve four degrees of freedom (DOF) for each node, making the computation very expensive. Moreover, solution of Navier-Stokes equations in the pipe requires to adopt, along the pipe walls, a mesh with dense element distribution in the normal direction (boundary layer mesh), thus increasing the overall number of elements. However, what plays a major role in the number of elements required for the discretization of the pipe is its high aspect ratio, with its cross-area much smaller than its length.

3.1 Reduction of the degrees of freedom

Many authors (see [7],[8] and [13]) modelled the flow in the pipe as a Hagen–Poiseuille flow, that is one-dimensional laminar flow through a tube. This approach is correct if the following assumptions hold:
- the component of the velocity perpendicular to the walls of the pipe is null;
- the components of the velocity parallel to the walls vanish on the walls (no-slip condition).

Studying the flow at the interface between free fluid and a porous matrix, Levy and Sanchez-Palencia [14] (in [10]) found that the velocity in the free fluid is much larger than the Darcy velocity in the porous matrix and, as a first approximation, the flow around the porous medium is the same as if the body were impervious. A more detailed investigation in the vicinity of the interface revealed the existence of an intermediate layer of thickness equal to the characteristic length of the matrix pores, which allows the asymptotic matching of the free fluid with the flow in the porous body. The assumptions therefore involve a negligible approximation.

Hagen–Poiseuille flow in tubes of general shape is described by the following equation:

$$U = -\frac{2D_h^2}{\beta\mu}\rho g \frac{\Delta H}{L} \qquad (5)$$

where U is the average velocity across the section, L is the length of the tube, β is a friction factor depending on the shape of the section (see Table 1) and D_h is named hydraulic diameter and is a ratio between the area of the section and its wetted perimeter ($D_h = 4A/P$).

By comparing eq.(5) with eq. (1) it's clear that Hagen–Poiseuille flow can be described by Darcy's law if a fictitious permeability is used:
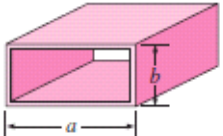
$$\kappa^* = \frac{2D_h^2}{\beta} \qquad (6)$$

When the cross section of the tube is elongated, with the thickness much smaller than the width ($a/b \rightarrow \infty$) as for the pipes observed in lab tests, we obtain

$$\kappa^* = \frac{b^2}{12} \qquad (7)$$

Table 1. Friction factor for different tube geometries.

Tube geometry	a/b	β
Circle	-	64.00
Rectangle	1	56.92
	2	62.20
	3	68.36
	4	72.92
	6	78.80
	8	82.32
	∞	96.00

and the flow in the pipe is given by

$$Q = -\frac{\rho g}{\mu}\frac{b^3 a}{12}\frac{\Delta H}{L} \qquad (8)$$

Formula (8) is the well known cubic law that describes flow in fractures [15].

If Hagen–Poiseuille flow is assumed to occur in the pipe, Darcy's law can be solved in the whole domain by assigning a fictitious permeability in the pipe as given by (6) or (7). In Darcy's law only a single unknown (pressure or hydraulic head) is associated to each node and the solution of the system of equations is much cheaper.

3.2 Reduction of the number of elements

In order to simplify the discretization of geometries with a high aspect ratio COMSOL features the Fracture Flow interface. The fracture (in this case the piping channel) is represented as a 2D (internal or external) boundary rather than a 3D domain (or a 1D boundary rather than a 2D domain, in two-dimensional modelling).

The following form of Darcy's law is solved in the fracture/pipe:

$$\mathbf{q}_f = -\frac{\kappa_f}{\mu}b(\nabla_\mathrm{T} p + \rho g \nabla_\mathrm{T} z) \qquad (9)$$

where, $\mathbf{q}_f$ is the volume flow rate per unit width in the fracture and ∇_T denotes the gradient operator restricted to the fracture tangential plane. The fracture permeability κ_f can be determined according to eq. (6) or (7). The specific discharge is considered constant across the depth of the fracture.

4. Physical and numerical model

For the lab experiment a sand sample is prepared in a box covered by a transparent plate. The sand is held between two vertical filters and a hydraulic head difference is applied between the inlet and the outlet of the water flow. The seepage length L is 0.32 m. The vertical filter at the outlet does not fully extend up to the covering plate so as to allow the sand grains at the interface with the cover to be removed by the seepage forces. Figure 2 illustrates the set-up.
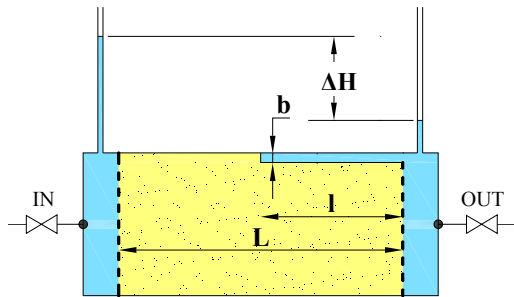
Figure 2. Set-up of the lab experiment.

The numerical model reproduces a sand sample where a pipe is present at the interface between the sand and the covering plate. We run steady state analyses, fixing in time the moment when the pipe, after having formed at the outlet and grown backwards, has reached a length l equal to half the seepage length. The pipe cross-section is constant along the length. The hydraulic head difference between inlet and outlet is imposed on the basis of the critical head measured in lab tests by other authors [4]. Characteristic parameters are reported in Table 2.

Both 2D and 3D analyses are performed. In the 2D model the pipe is idealized as a slot that extends to infinity in the third direction. In the 3D model (Figure 3 and 4) the pipe is modelled as a channel situated at the center of the box. The symmetry of the problem allows us to model only half the box and half the pipe.

We compare the modelling approaches described in section 2, moving from the most accurate but also most expensive to the most simplified. Table 3 gives an overview of the COMSOL interfaces used.

Table 2. Geometrical parameters and material properties.

Parameter		Value	
Seepage length	L	0.32	m
Pipe length	l	0.16	m
Pipe thickness	b	0.0018	m
Pipe width	a	0.010	m
Matrix porosity	n	0.40	
Matrix permeability	κ	1.6e-11	m^2
Hydraulic load	ΔH	0.10	m

Table 3. List of COMSOL interfaces used and corresponding equations solved.

COMSOL interface	Equation solved	
	Matrix	**Pipe**
Free and porous media (FPM)	Brinkman	Navier-Stokes
Darcy's law (DL)	Darcy	Darcy
Darcy's law + Fracture flow (DL+FF)	Darcy	Darcy (FF formulation)

In the model that adopts the Free and porous media interface (FPM) a pressure boundary condition is defined at the inlet and the outlet of the domain, together with the condition of zero viscous stress. Along the impermeable walls the 'no slip' condition is applied ($\mathbf{u} = 0$) while on the symmetry plane (3D model) the symmetry boundary condition prescribes no flow penetration and vanishing shear stress. At the interface between the porous matrix and the pipe the implemented boundary condition enforces continuity for the velocity field and for the pressure. We use piecewise quadratic triangles for the velocity components and piecewise linear triangles for the pressure (P2-P1 finite elements).

In the models that adopts the Darcy's law and Fracture flow interface (DL and DL+FF) the hydraulic head is defined at the inlet and the outlet of the domain. Continuity of the pressure is enforced on the internal boundaries. Models adopting piecewise quadratic (P2) and piecewise linear (P1) triangles are compared.
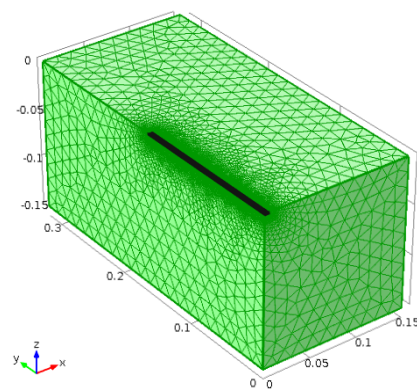

Figure 3. 3D numerical model: the dark area corresponds to the pipe. The discretization is much finer in the pipe and its surroundings.
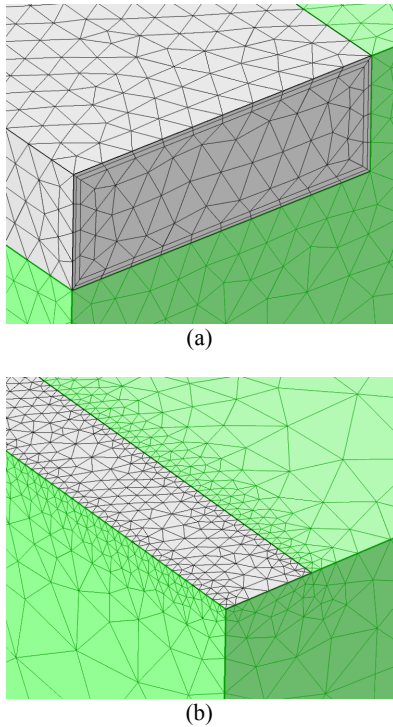
(a)

(b)

Figure 4. Details of the discretization: the pipe is modelled as a 3D domain in the Free and porous media and Darcy's law interface (a) and as a 2D domain in the Fracture flow interface (b); in FPM two layers of boundary elements have been used.

5. Numerical results and discussion

The piping channel acts as a drain and water flows from the porous matrix towards the pipe, entering both at the head and at the bottom of the pipe. Figure 5 shows the flow net under the piping channel. The deeper the sand layer the more the water entering at the bottom. However a value D_{lim} can be defined, above which the flow to the pipe is no longer influenced by a further increase in the depth D of the sand layer.
The pipe can be thought of as a region of the domain of high permeability and, consequently, low hydraulic resistance. Therefore most energy is dissipated upstream of the pipe and only a very small amount of energy is dissipated in the pipe. The flow velocity in the pipe is some orders of magnitude higher than in the porous matrix and slightly increases towards downstream, as a consequence of the water entering all along the pipe length (Figure 6). This velocity increase also occurs since the cross-

section of the pipe, for the sake of simplicity, has been set constant along the length. Lab experiments show however that the cross-section enlarges towards downstream, due to increasing erosion potential. The values of the physical quantities represented in Figure 6 are strongly dependent on the thickness of the pipe.
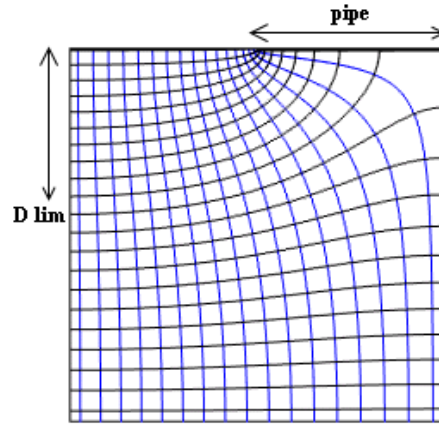

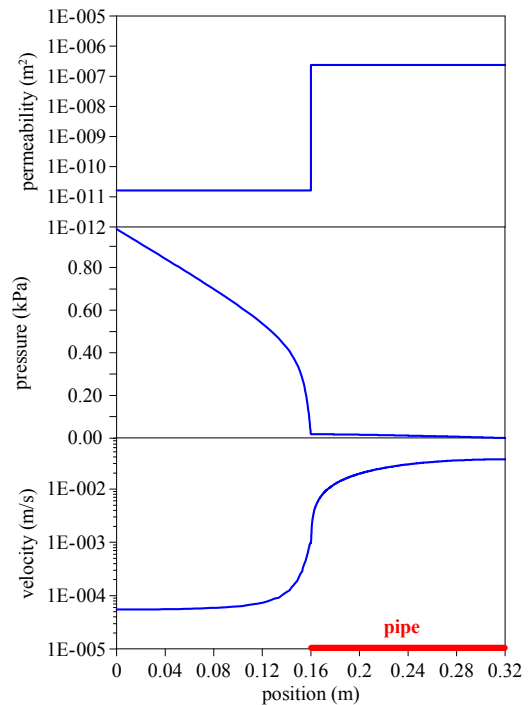**Figure 5.** Flow net under a piping channel.

Figure 6. Permeability, water pressure and flow velocity along the seepage path at the top of the sand layer, at the position where the pipe develops.

5.1 Comparison of modelling approaches

A summary of the mesh characteristics of the numerical models developed is presented in Table 4. For each model the total flow in the pipe is evaluated in a section close to the exit point and the variation with respect to the most accurate model, that is the one that makes use of the FPM interface, is reported in the table.

We observe that moving from FPM to DL interface the degrees of freedom are reduced. The number of elements also slightly reduces as boundary layers are no longer needed and first order elements can be adopted. By modelling the pipe with the FF interface we have the possibility to considerably reduce the number of elements in the pipe and its surroundings. No relevant difference exists among the results of the FPM and DL interface, despite it has been observed that the hypothesis of parallel flow in the pipe is not satisfied at the head of the pipe.

Some discrepancies arise using the FF interface, which decrease if the mesh is coarsened.

By varying the depth of the sand layer with a parametric sweep, we observe that the flux in the pipe obtained with FF interface is underestimated of an amount that increases with the depth of the sand layer up to D_{lim} and remains constant after a further increase of the depth. The increase of the error follows the same trend of the increase of the flux at the exit of the pipe (Figure 7).

Table 4. List of numerical models compared, mesh characteristics and error respect to FPM interface.

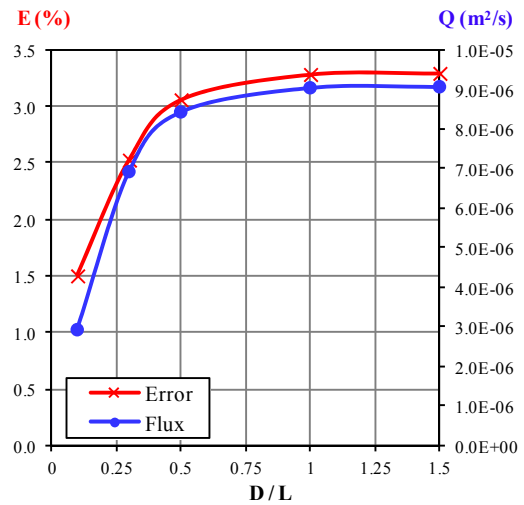| Inter-face	Elem. Type	N. Elem.	N. DOF	E %
2D				
FPM	P2+P1	10.3k	53k	0.0
DL	P2	8.7k	18k	0.1
DL	P1	8.7k	4.6k	0.2
DL+FF	P1	8.7k	4.6k	-3.5
DL+FF	P1	1.3k	2.7k	-3.3
3D				
FPM	P2+P1	467k	2536k	0.0
DL	P2	122k	177k	0.2
DL	P1	122k	24k	1.5
DL+FF	P1	77k	16k	-11.2
DL+FF	P1	22.7k	4.8k	-2.8

Figure 7. Error committed using the Fracture Flow interface and flux at the exit of the pipe for increasing (normalized) depth of the sand layer.

5.2 Influence of the boundaries

We investigated the influence exerted on the flow field by the walls of the box, as they constitute a limit to the flow in comparison with the field condition. This was achieved by varying the thickness D and semi-width B of the sand box with a parametric sweep.

Figure 8.a shows the variation of the hydraulic head induced by the presence of the pipe, normalized with reference to the undisturbed head:

$$\Delta H_{rel} = \frac{H(x,y,z) - H_0(x,y,z)}{H_0(x,y,z)} \quad (10)$$

The size of the model is $D=B=L=0.32$m. The red contour delimits the volume outside which the decrease of the hydraulic head is lower than 5% of the undisturbed value.

The volume affected by the presence of the pipe is axisymmetric around the pipe axis only if the depth of the sand layer is larger than D_{lim} as in Figure 8.a. Figure 8.b shows the variation of the hydraulic head induced by the pipe for a sand layer with thickness $D=0.2L$. The area influenced by the pipe spreads laterally: more water is beckoned by the pipe from the sides, since it is not available from the bottom.

Figure 9 illustrates how the error generated by the presence of the lateral walls diminishes as the size of the box increases. The error is calculated as the variation of pressure drop in the
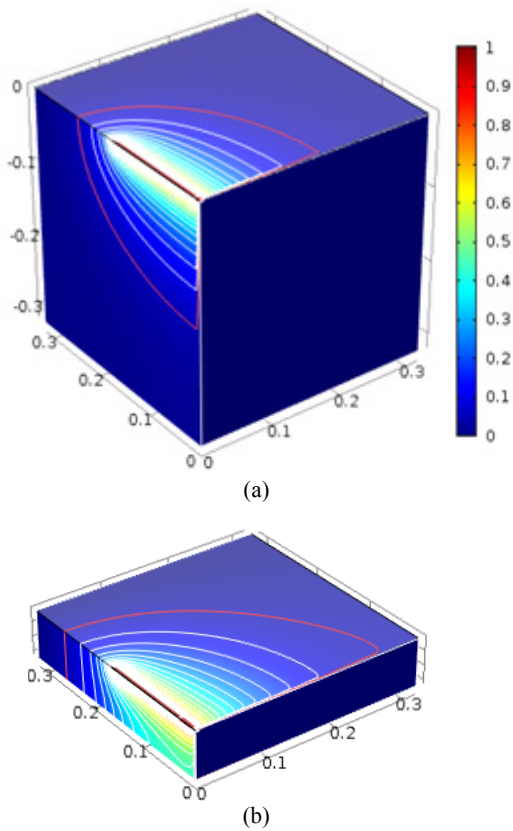
(a)

(b)

Figure 8. Relative variations of the pressure induced by the presence of the pipe for different depths of the sand layer: *D=L* (a) and *D=0.2L* (b). The red curve indicates a 5% variation.
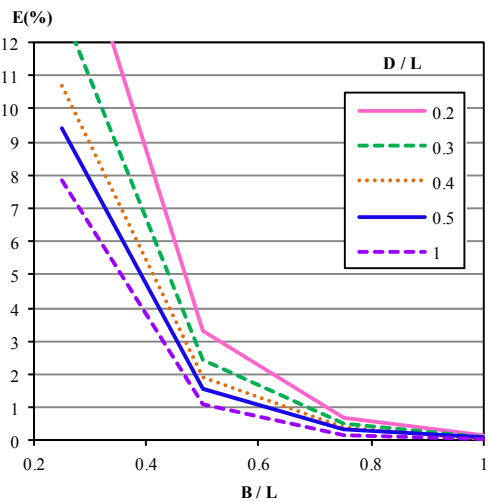

Figure 9. Error generated by close boundaries as function of normalized semi-width *B* and depth *D* of the box.
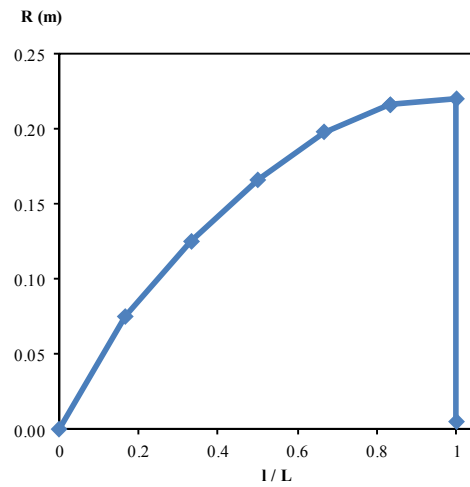

Figure 10. Radius of influence of the pipe as function of the normalized length of the pipe.

pipe with respect to the case of far boundaries. The error is lower than 2% if $B=D>0.5L$.

It was also investigated how the radius of influence varies as the length of the pipe increases (Figure 10). The radius of influence is defined as the maximum distance from the pipe beyond which the drop in hydraulic head is lower than 5% of the undisturbed value. When the pipe reaches upstream the sudden pressure rise in the pipe causes the radius of influence to fall down up to the value of the radius of the pipe itself, because the pipe does not act anymore as a drain.

6. Conclusions

Our work shows that laminar flow in piping channels can be modelled in COMSOL with a limited computational effort by using Darcy's law. The permeability assigned in the pipe should be derived from the cubic law, if the cross-section of the pipe is elongated, or, more generally, from the Poiseuille formula. However the high aspect ratio of the geometry requires many elements to discretize the pipe and its surroundings, especially when modelling real, full-scale structures. To overcome this problem the performance of the Fracture flow interface has been tested. The Fracture flow interface underestimates the flow in the pipe if a fine mesh is used along the pipe, but the performance improves by increasing the size of the mesh.

7. References

1. C. F. Wan and R. Fell, Investigation of rate of erosion of soils in embankment dams, *Journal of Geotechnical and Geoenv. Eng.*, vol. **130** (**4**), pp. 373-380 (2004).
2. J. K. Vrijling, Piping - Realiteit of Rekenfout?, Rijkswaterstaat, Waterdienst (2010) [in Dutch].
3. M. Foster, R. Fell and M. Spannangle, The statistics of embankment dam failures and accidents, *Canadian Geotech. Journal*, vol. **37**, pp. 1000-1024 (2000).
4. V.M. van Beek, J.G. Knoeff and J.B. Sellmeijer, Observations on the process of piping by underseepage in cohesionless soils in small-, medium- and full-scale experiments, *European Journal of Environmental and Civil Engineering*, vol. **15** (**8**), pp. 1115-1138 (2011).
5. Y. L. Beck et al., Thermal Monitoring of Embankment Dams by Fiber Optics, *8th ICOLD European Club Symposium*, pp. 444-448 (2010).
6. M.A. Mooney et al., Design and Implementation of Geophysical Monitoring and Remote Sensing during a Full Scale Embankment Internal Erosion Test, *2014 GeoCongress* (to be published).
7. J.B. Sellmeijer, Numerical computation of seepage erosion below dams (piping), 3rd Int. Conf. on Scour and Erosion, pp. 596-601 (2006).
8. J.M. van Esch et al., Modeling Transient Groundwater Flow and Piping under Dikes and Dams, *3rd International Symposium on Computational Geomechanics (ComGeo III)* (2013)
9. K. Vandenboer, V. van Beek and A. Bezuijen, Physical erosion mechanism of the progression of backward erosion piping, *21st annual meeting of EWGIE* (2013).
10. M. Discacciati and A. Quarteroni, Navier-Stokes/Darcy Coupling: Modeling, Analysis and Numerical Approximation, Revista Matematica Complutense, vol. **22**, pp. 315–426 (2009).
11. H.C. Brinkman, A calculation of the viscous force exerted by a flowing fluid on a dense swarm of particles, *Appl. Sci. Res.*, vol. **A1**, pp. 27-34 (1947).
12. S. Whitaker, The method of volume averaging, Kluwer Academic Publishers, Dordrecht, The Netherlands (1999).
13. G. Hoffmans, Personal communication.
14. T. Levy and E. Sanchez-Palencia, On the boundary conditions for fluid flow in porous media, *Int. J. Eng. Science*, vol. **13**, pp. 923–940 (1975).
15. P. A. Witherspoon at al., Validity of the cubic law for fluid flow in a deformable rock fracture, *Water Resources Research*, vol. **16**(**6**), pp. 1016-1024 (1980).